

Absorption Spectrum and Kinetics of the Acetylperoxy Radical

Coleen M. Roehl,* Dieter Bauer, and Geert K. Moortgat*

Max-Planck-Institut für Chemie, Atmospheric Chemistry Division, Postfach 3060, 55020 Mainz, Germany

Received: September 6, 1995; In Final Form: December 4, 1995[⊗]

The ultraviolet absorption spectrum of acetylperoxy radical was remeasured in the 195–280 nm range. Acetylperoxy radicals were generated by laser flash photolysis of Cl₂/CH₃CHO/O₂ mixtures. The absorption cross sections were calibrated against the ethylperoxy radical, generated in the flash photolysis of Cl₂/C₂H₆/O₂ mixtures. The acetylperoxy spectrum is bimodal, with a strong maximum at 207 nm, $\sigma = 6.67 \times 10^{-18}$ cm² molecule⁻¹, and a weaker maximum near 240 nm, $\sigma = 3.21 \times 10^{-18}$ cm² molecule⁻¹. Newly obtained cross sections were used along with absorption–time profiles, obtained over a range of radical concentrations, to determine a rate constant for the acetylperoxy self reaction at 298 K, $2\text{CH}_3\text{C}(\text{O})\text{O}_2 \rightarrow 2\text{CH}_3\text{C}(\text{O})\text{O} + \text{O}_2$, of $k_1 = (1.36 \pm 0.19) \times 10^{-11}$ cm³ molecule⁻¹ s⁻¹, and to determine the rate coefficients for the acetyl- and methylperoxy cross reactions at 298 K, $\text{CH}_3\text{C}(\text{O})\text{O}_2 + \text{CH}_3\text{O}_2 \rightarrow \text{CH}_3\text{C}(\text{O})\text{O} + \text{CH}_3\text{O} + \text{O}_2$ and $\text{CH}_3\text{C}(\text{O})\text{O}_2 + \text{CH}_3\text{O}_2 \rightarrow \text{CH}_3\text{C}(\text{O})\text{OH} + \text{HCHO} + \text{O}_2$, of $k_{4a} = (8.8 \pm 1.5) \times 10^{-12}$ cm³ molecule⁻¹ s⁻¹ and $k_{4b} = (1.0 \pm 0.5) \times 10^{-12}$ cm³ molecule⁻¹ s⁻¹, respectively. New cross sections are reported for CH₃O₂ and HO₂ and the absorption spectrum of CH₃COCl is presented.

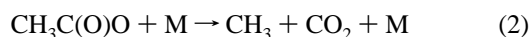
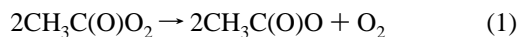
Introduction

Following the discovery of the role of peroxy radicals in balancing the photostationary state of NO_x/O₃ in polluted environments, extensive studies of oxidative degradation processes of hydrocarbons in the atmosphere have been undertaken.¹ Acetylperoxy radicals, in particular, are known to be formed in the photooxidation of higher carbonyl compounds (i.e., acetaldehyde, acetone, methyl vinyl ketone, methylglyoxal, etc.) and, hence, are important in many atmospheric photooxidation processes. CH₃C(O)O₂ is also a precursor to peroxy-acetyl nitrate (PAN), which acts as a temporary reservoir and transporter for NO_x within cooler regions of the troposphere.^{2,3} Furthermore, thermal decomposition of PAN is believed to be a significant source of nighttime peroxy radicals, which take part in the important RO₂ + NO₃ nighttime chemistry.⁴ Finally, peroxy radical self and cross reactions become important in NO_x-free or clean environments. For example, the cross reaction between acetylperoxy radicals and HO₂ is thought to be responsible for the significant organic acid buildup in the troposphere.^{5,6} Yet, despite its atmospheric importance, the spectrum and kinetics of the acetylperoxy radical are not well established.

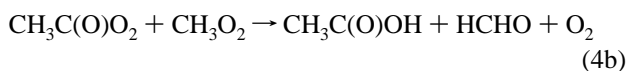
The UV absorption spectrum of the acetylperoxy radical was first determined in a modulated photolysis study by Addison *et al.*⁷ Cl₂/CH₃CHO/O₂/NO₂ mixtures were photolyzed to generate the radicals and the formation of PAN was observed. The CH₃C(O)O₂ spectrum was obtained by correcting the composite spectrum for contributions due to PAN and by subtracting the components due to CH₃O₂. In two newer studies, the acetylperoxy radicals were produced by flash photolysis of Cl₂/CH₃CHO/O₂ mixtures. Basco and Parmar⁸ did an absolute calibration by measuring the amount of chlorine dissociated in the flash. Moortgat *et al.*⁹ measured the absorption cross sections relative to the absorption cross section of HO₂ at 210 nm. Although the general shapes of the three spectra are the same, the magnitudes of the two maxima are not in agreement. The best available acetylperoxy spectrum is the Moortgat *et al.*⁹ data rescaled (downward 21 and 14%, respectively) to

account for a subsequent redetermination of the HO₂ cross section at 210 nm, as recommended by two recent organic peroxy radical reviews.^{10,11} However, since Moortgat *et al.*⁹ used computer simulations, which utilized the erroneously high HO₂ cross sections, to fit absorbance traces and to concurrently optimize both the CH₃C(O)O₂ cross section and the CH₃C(O)O₂ self reaction rate constant, such a simple rescaling is not adequate.

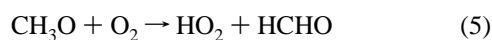
Determinations of the kinetic parameters for the acetylperoxy system have been based on concentration profiles calculated from measured absorbances using the available cross sections. Hence, discrepancies in the CH₃C(O)O₂ cross sections have, in part, also created large differences in the calculated reaction rate constants. CH₃C(O)O₂ is not the only absorbing species present during such measurements; CH₃O₂ and HO₂ radicals grow in as CH₃C(O)O₂ decays. CH₃C(O)O₂ radicals self react quickly according to reaction 1. The resulting CH₃C(O)O radicals then undergo rapid thermal decomposition^{12,13} to yield methyl radicals, which add O₂ to produce CH₃O₂:



Besides self reacting, the two peroxy radicals also react with each other via

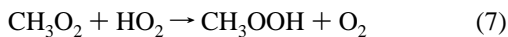


The methoxy radicals, CH₃O, generated in reaction 4a further react with the excess O₂ via



to form HO₂ radicals. And finally, HO₂ radicals also undergo self reactions and reactions with CH₃C(O)O₂ and CH₃O₂:

[⊗] Abstract published in *Advance ACS Abstracts*, February 15, 1996.



Addison *et al.*⁷ analyzed their modulated absorption curves as a function of time to obtain the rate constants $k_1 = (2.5 \pm 1.0) \times 10^{-12} \text{ cm}^3 \text{ molecule}^{-1} \text{ s}^{-1}$ and $k_4 = 3.0 \times 10^{-12} \text{ cm}^3 \text{ molecule}^{-1} \text{ s}^{-1}$ ($k_4 = k_{4a} + k_{4b}$). Basco and Parmar⁸ calculated a larger k_1 value of $(8.0 \pm 1.5) \times 10^{-12} \text{ cm}^3 \text{ molecule}^{-1} \text{ s}^{-1}$ from second-order fits of decay traces obtained near 200 nm. Rate constants of $k_1 = (1.7 \pm 0.4) \times 10^{-11}$ and $k_4 = (1.4 \pm 0.3) \times 10^{-11} \text{ cm}^3 \text{ molecule}^{-1} \text{ s}^{-1}$ and a branching ratio of $\alpha = k_{4a}/k_4 = 0.48$ at 298 K were deduced from the computer simulations of Moortgat *et al.*⁹ A strong temperature dependence in the CH₃C(O)O₂ + CH₃O₂ branching ratio was noted by Moortgat *et al.*⁹ and led to a further study¹⁴ of the products and branching ratio between 223 and 333 K. The temperature dependence of the cross reactions was determined to be $\beta = k_{4a}/k_{4b} = 2.2 \times 10^6 \exp(-3870/T)$, yielding $\alpha = \beta/(1 + \beta) = 0.83 \pm 0.17$ at 298 K in contradiction to their earlier measurement. Since our work began, another flash photolysis experiment¹⁵ was initiated to study k_4 . The CH₃O₂ radical precursor, CH₄, was added to the photolysis mixtures of Cl₂/CH₃CHO/O₂ and the radical concentrations were monitored by UV absorption. Preliminary reports give $k_4 = (7.6 \pm 3.8) \times 10^{-12} \text{ cm}^3 \text{ molecule}^{-1} \text{ s}^{-1}$ at 298 K using $\alpha = 0.48$.

In an attempt to resolve the existing discrepancies in the absorption spectrum of acetylperoxy radical and in the kinetic parameters, especially the CH₃C(O)O₂ + CH₃O₂ branching ratio, a new laser flash photolysis experiment was constructed and employed. A new ultraviolet absorption spectrum of acetylperoxy radical is reported in the 195–280 nm range. The rate coefficients for the acetylperoxy self reaction and cross reaction with methylperoxy were determined at 298 K from absorption–time profiles using the newly obtained cross sections.

Experimental Section

For all experiments described here, CH₃C(O)O₂ radicals were generated by laser flash photolysis of Cl₂, using the 351 nm XeF line of a Lambda Physik LPX-300 excimer laser, in the presence of CH₃CHO and O₂ via the reactions



Methylperoxy radicals, CH₃O₂, evolved as secondary products of the rapid self reaction of acetylperoxy radicals according to reactions 1–3. In some experiments, CH₄ was added to the photolysis mixtures and CH₃CHO was reduced in order to generate initial CH₃O₂ radicals and thereby enhance the reaction flux through the cross reaction channels, reactions 4a and 4b. This initial CH₃O₂ is formed from the reactions



The respective precursor concentrations were adjusted according to their rate constants with Cl to ensure that complete conversion to CH₃C(O)O₂ and CH₃O₂ occurred. (See Results.)

The light intensity from a deuterium (D₂, Hamamatsu) probe lamp passing through the photolysis cell was monitored, before (I_0) and at known times after the flash (I_t), at specific wavelengths. Attenuation of this light beam upon production of absorbing radicals was used to calculate the absorbance at that wavelength (λ) as a function of time with the equation

$$\text{Abs}_{\lambda,t} = -\ln[I_t/I_0] \quad (A)$$

The absorbances were converted into cross sections, $\sigma_\lambda(i)$, using the Beer–Lambert relationship

$$\sigma_\lambda(i) = \text{Abs}_{\lambda,t} / (l[i]_t) \quad (B)$$

where l is the pathlength and $[i]_t$ is the concentration of a single absorbing species, i , at time, t . Once measured, the cross sections of acetylperoxy, along with the Beer–Lambert equation for a multiabsorber system,

$$\text{Abs}_{\lambda,t} / l = \sum_n \sigma_\lambda(i)[i]_t \quad (C)$$

were used to convert absorption–time profiles to absorber concentration–time profiles (n is the number of absorbers). A simulation program was thereafter employed to fit the measured absorbances and to simulate concentration–time profiles, thus deriving information on the kinetics of the radicals involved.

The apparatus used in these experiments is shown in Figure 1. A rectangular quartz cell of 40 cm length was used, and photolysis was performed from the side by expansion of the output from the pulsed excimer laser with a set of cylindrical mirrors. The light from the D₂ lamp was passed lengthwise through the cell and was folded by internal White optics, resulting in eight passes with a total path length of 326 cm, before it entered a 0.5 m monochromator (Acton Research Corporation, grating with 300 lines mm⁻¹ blazed at 300 nm), which was equipped with both a photomultiplier tube (PMT, Hamamatsu) and a gated photodiode array detector (EG&G Princeton Applied Research). The entrance slit of the monochromator and the slit between the monochromator and the PMT were fixed at 0.5 mm, resulting in a PMT resolution of about 3.3 nm. The photodiode array resolution, calculated as the full width at half-maximum FWHM of the 282.4 nm line of the Zn lamp, was 1.0 nm. All experiments were conducted at or near 298 K.

The gated photodiode array detector was used to measure relative cross sections over the entire spectral region between 195 and 280 nm within a small time window. The gate timing of the photodiode array measurements, or the time during which light impinged on the diode array, was established by preset pulses sent by the delay generator with typical duration times of $\sim 10 \mu\text{s}$. Measurements consisted of the coaddition of multiple scans (~ 5000) taken both immediately before (I_0) and over the time period between 1 and 11 μs after the laser pulses (I_t). The wavelength scale was calibrated with an accuracy of $\sim 0.2 \text{ nm}$ with the output from a Zn lamp.

Single wavelength absorption measurements, used to determine both absorption cross sections and rate constants, were carried out as a function of time using the PMT. The output of the PMT, a small dc signal, was amplified, digitized, and transferred to a personal computer for analysis. As with the photodiode array measurements, I_0 was obtained by averaging the PMT signal immediately before the laser pulse. The I_t values were typically recorded between 0 and 4 ms after the laser flash with a 5 μs resolution and between 4 ms and 2 s after the laser flash with a 50 μs resolution. The final absorption–time profiles

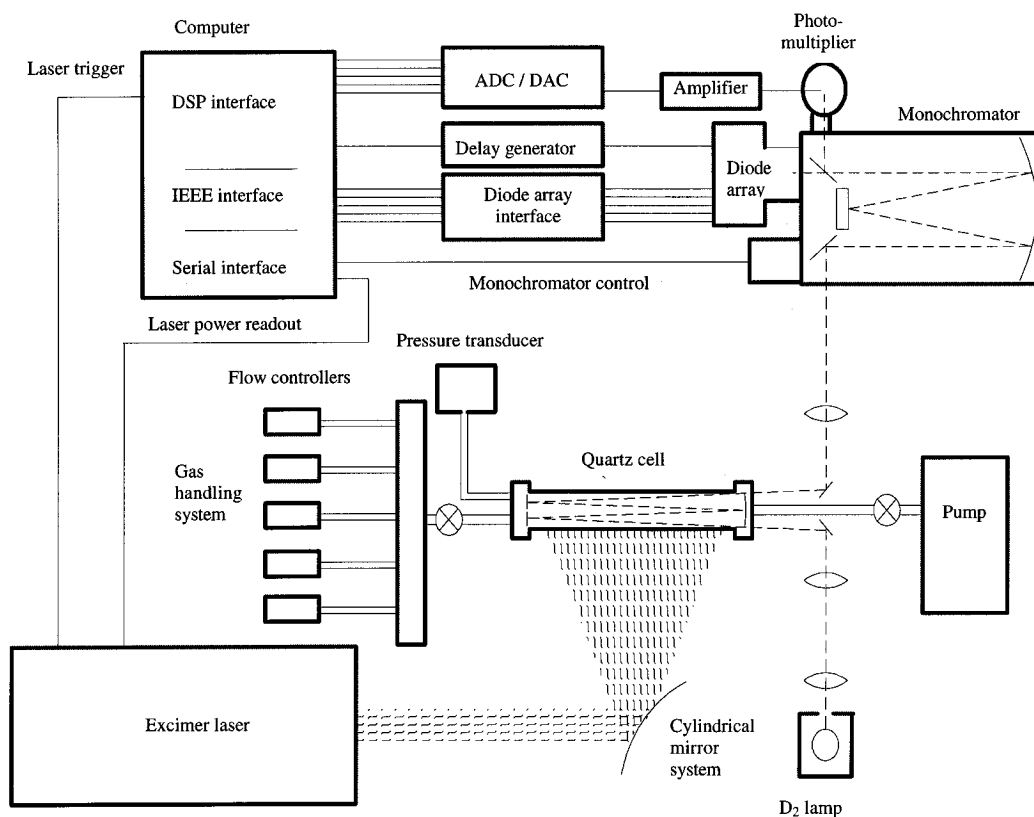


Figure 1. Schematic diagram of the instrument used in the $\text{CH}_3\text{C}(\text{O})\text{O}_2$ absorption cross sections and kinetic experiments.

usually consisted of averaged signals of three or four sets of 500 laser pulses. When relative wavelength measurements were made, the wavelength was alternated after each set of 500 flashes.

The Cl_2 , O_2 , N_2 bath gas and in certain experiments CH_4 , C_2H_6 , or gaseous CH_3CHO were introduced through calibrated mass flowmeters. For higher acetaldehyde concentrations, an additional regulated flow of N_2 was bubbled through liquid CH_3CHO which was contained in a temperature-controlled vessel. The CH_3CHO temperature and N_2 flow were varied to attain a suitable CH_3CHO concentration. With total pressures of ~ 400 Torr and flow rates between 4000 and 5000 sccm, the residence time in the cell was about 5–6 s. The repetition rate of the laser was greater than or equal to the residence time, thus ensuring that the photolysis products formed in one laser flash were flushed out and that a fresh gas mixture was flowed into the cell before the next laser flash. The stated purities of the compounds used were Cl_2 , 99.95% in a 1.0% mix in 99.999% N_2 ; O_2 , 99.99%; N_2 , 99.999%; CH_3CHO , 99%; CH_4 , 99.995%; and C_2H_6 , 99.95%.

Results

In this work, several parameters were obtained: the UV absorption cross sections of $\text{CH}_3\text{C}(\text{O})\text{O}_2$, the rate constant for the self reaction of $\text{CH}_3\text{C}(\text{O})\text{O}_2$, and the reaction rate constant of $\text{CH}_3\text{C}(\text{O})\text{O}_2 + \text{CH}_3\text{O}_2$ along with its branching ratio. During the course of this study, the spectra of $\text{CH}_3\text{C}(\text{O})\text{Cl}$, CH_3O_2 , and HO_2 were also measured.

Absorption Cross Sections. Absorption cross sections of $\text{CH}_3\text{C}(\text{O})\text{O}_2$ were measured using both the PMT and the gated photodiode array systems. For each of these measurements, the initial radical concentration and therefore the initial decay rate were minimized by photolyzing only small amounts of Cl_2 . Cl_2 concentrations of $(2-3) \times 10^{16}$ molecule cm^{-3} were employed and typically $[\text{Cl}]_i = (2-3) \times 10^{13}$ molecule cm^{-3}

were produced per laser pulse. CH_3CHO concentrations were kept high, about $(1-3) \times 10^{17}$ molecule cm^{-3} . O_2 addition to $\text{CH}_3\text{C}(\text{O})$ was ensured by maintaining high O_2 concentrations of about $(8-9) \times 10^{18}$ molecule cm^{-3} , and the maximum $\text{CH}_3\text{C}(\text{O})\text{O}_2$ radical concentration was achieved within $< 1 \mu\text{s}$. Preventing significant buildups of $\text{CH}_3\text{C}(\text{O})$ is important since it is known to have large cross sections with a maximum of about 3.8×10^{-17} cm^2 molecule $^{-1}$ at 216 nm.⁸ High O_2 concentrations also minimized the $\text{CH}_3\text{C}(\text{O}) + \text{Cl}_2$ reaction forming acetyl chloride ($\text{CH}_3\text{C}(\text{O})\text{Cl}$). An absorbance spectrum of this product, displaying a maximum near 240 nm, was recorded by Basco and Parmar;⁸ however, cross sections were not reported. Since $\text{CH}_3\text{C}(\text{O})\text{Cl}$ is a stable molecule which would continue to absorb even after the radical concentrations had been greatly reduced, its existence could lead to errors in the kinetic analysis. The significance of $\text{CH}_3\text{C}(\text{O})\text{Cl}$ absorption in this system depends on the magnitude of the $\text{CH}_3\text{C}(\text{O})\text{Cl}$ cross sections relative to those of the peroxy radicals. For this reason, UV spectra of 0.9–1.6 Torr samples of pure $\text{CH}_3\text{C}(\text{O})\text{Cl}$ were measured in a static system using the photodiode array detector. Results given in Figure 2 show that $\text{CH}_3\text{C}(\text{O})\text{Cl}$ absorbs only weakly in the wavelength range of interest, with a maximum of 1.30×10^{-19} cm^2 molecule $^{-1}$ at 241 nm. $\text{CH}_3\text{C}(\text{O})\text{Cl}$ cross sections, given as squares in Figure 2, were also calculated from the absorbance spectrum of Basco and Parmar⁸ and were normalized to our value at 240 nm. Under our experimental conditions, no evidence of either $\text{CH}_3\text{C}(\text{O})$ at short time scales or $\text{CH}_3\text{C}(\text{O})\text{Cl}$ at long time scales was observed.

To avoid doing complex spectral subtractions of secondary absorbing species, CH_3O_2 and HO_2 , it was necessary to measure the $\text{CH}_3\text{C}(\text{O})\text{O}_2$ spectrum immediately upon formation. O_3 , produced in reaction 6b, also absorbs in the wavelength region of interest, but its concentration and hence its contribution to the total absorbance was negligible throughout the time period analyzed. The ability to record the entire spectrum in a very

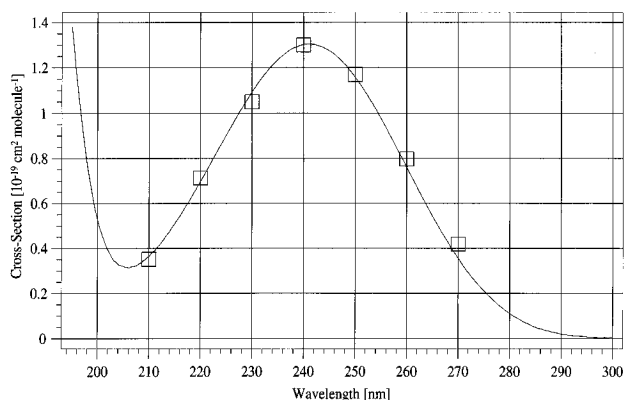


Figure 2. UV absorption cross sections of CH₃C(O)Cl measured near 298 K. This work is shown as the solid line; squares represent cross sections calculated from the absorbance spectrum of ref 8 and normalized to our value at 240 nm.

short time interval (1–11 μ s) was achieved by the combination of using a relatively large setting for the entrance slit of the monochromator and the gated photodiode array detector. On average, only about 0.5% of the CH₃C(O)O₂ decayed during this short measurement time interval, and therefore significant concentrations of secondary absorbers were not produced during the measurement. The shape of the spectral feature was calculated with eq A.

The UV absorption features were also mapped out in 10 nm intervals through repeated determinations of $Abs_{\lambda,0}/Abs_{240nm,0}$ with the PMT system. The absorbance values at time $t = 0$ were obtained by extrapolating second order fits of the measured absorption–time profiles, extending out to times of ~ 1 ms, back to zero time. Because of secondary chemistry, fits of these absorption–time profiles (as such) cannot be used to derive information about the decay rate of CH₃C(O)O₂. However, they can be used to determine the initial CH₃C(O)O₂ absorbance. At $t = 0$, no absorbing products have yet been formed and the extrapolated absorbances are only due to CH₃C(O)O₂.

Calculating the absolute UV absorption cross sections of CH₃C(O)O₂ from either the photodiode array or the PMT absorbance values requires knowledge of the concentration of CH₃C(O)O₂ present at the time of the measurement. The CH₃C(O)O₂ concentration depends on the Cl atom concentration formed in the photolysis flash, which in turn is determined by the Cl₂ concentration and the laser intensity. Due to the difficulty in accurately measuring the absolute laser intensity, the Cl atom concentrations (and therefore the CH₃C(O)O₂ concentrations) were instead calibrated against the ethylperoxy radical, which was generated in separate flash photolysis experiments of Cl₂/C₂H₆/O₂ mixtures. CH₃C(O)O₂ and C₂H₅O₂ absorption measurements were made back-to-back at 240 nm with the PMT, and initial absorbances were calculated by the extrapolation technique described above. Care was taken to maintain the same Cl₂ concentrations and relative laser power in the two measurements, so that the Cl atom concentrations and, hence, the initial peroxy radical concentrations were equal, $[CH_3C(O)O_2]_0 = [C_2H_5O_2]_0$. Small corrections (usually <3%) were made when changes in Cl₂ concentration and/or laser power did occur. By solving eq B for $[C_2H_5O_2]_0$ and $[CH_3C(O)O_2]_0$, setting these equations equal, and rearranging, the equation

$$\sigma_{240nm}(CH_3C(O)O_2) = \frac{Abs_{240nm,0}(CH_3C(O)O_2) \sigma_{240nm}(C_2H_5O_2)}{Abs_{240nm,0}(C_2H_5O_2)} \quad (D)$$

is derived for calculating the absorption cross section of CH₃C(O)O₂ at $\lambda = 240$ nm, where $Abs_{240nm,0}(CH_3C(O)O_2)$ and $Abs_{240nm,0}(C_2H_5O_2)$ are the extrapolated absorbances at $t = 0$ in the CH₃C(O)O₂ and C₂H₅O₂ systems, respectively. The C₂H₅O₂ cross section recommended by Lightfoot *et al.*¹⁰ ($\sigma_{240nm}(C_2H_5O_2) = (4.36 \pm 0.22) \times 10^{-18}$ cm² molecule⁻¹) is preferred over the 4.8% lower value of Wallington *et al.*¹¹ because its derivation included a more recent measurement performed in this laboratory.¹⁶ Since the publication of the reviews, Maricq and Wallington¹⁷ completed another study on C₂H₅O₂ cross sections in which they found $\sigma_{240nm}(C_2H_5O_2) = 4.6 \times 10^{-18}$ cm² molecule⁻¹, a value 5% higher than the Lightfoot review. A value of $\sigma_{240nm}(CH_3C(O)O_2) = (3.21 \pm 0.32) \times 10^{-18}$ cm² molecule⁻¹ was determined.

The single wavelength PMT absorption values and the photodiode array spectrum were normalized to the absorption cross section value determined at 240 nm and are displayed in Figure 3. As is observed in Figure 3, the ratio $R = \sigma_{210nm}/\sigma_{240nm}$ measured with the photodiode array detector is smaller than that from the PMT. Further investigations suggested that this ratio R determined with the photodiode array detector was dependent on the initial radical concentration. Photodiode array measurements were conducted in which the initial radical concentrations were stepwise reduced from 3×10^{13} to 7×10^{12} molecule cm⁻³, by decreasing the Cl₂ concentration and/or limiting the laser power. The ratio R calculated from the resulting spectra increased with decreasing radical concentration, approaching the ratio measured with the PMT. Extrapolating a plot of these ratios versus radical concentration back to zero initial radical concentration resulted in a ratio of 2.02, exactly equal to the PMT measured ratio. Test measurements of the C₂H₅O₂ spectrum, which has smaller cross sections in the low wavelength region, did not reveal a similar problem. These experiments suggested that large changes in the light intensity, occurring at short wavelengths, where the intensity from the D₂ lamp is drastically reduced, caused a nonlinearity problem in the photodiode array detector, resulting in erroneously low absorbances. Unfortunately, avoiding the nonlinearity hindrance by reducing the radical concentration results in a much noisier spectrum. To maintain the better signal-to-noise level, the photodiode array spectrum shown in Figure 3 was corrected by dividing it into smaller wavelength ranges and then recalculating the cross sections, scaling them to the PMT measurements in the same wavelength range. The final spectrum is given as the solid line in Figure 4 and the cross sections are reported in Table 1.

Error Analysis for the CH₃C(O)O₂ Cross Sections. In calculating the statistical error in the CH₃C(O)O₂ cross sections, the errors associated with the parameters in eq D were first considered. An error limit of 5% was used for $\sigma_{240nm}(C_2H_5O_2)$, based on the errors quoted in ref 16. The signal-to-noise ratios obtained from the averaged absorption profiles are sufficiently high such that errors in the extrapolations of these curves are expected to be 2–3% at 240 nm, increasing to 5% at 200 and 280 nm. Including the small errors ($\leq 1\%$) associated with the fluctuations in the laser power and Cl₂ concentration, statistical errors of 6% and 8% are calculated for the cross sections at 240 nm and at 200 and 280 nm, respectively. This error does not include systematic errors which may have evolved as a result of problems in the apparatus, the complete Cl atom to peroxy radical conversion, or secondary chemistry. Taking these into account, the total errors on the CH₃C(O)O₂ cross sections are estimated to be 10% at 240 nm and 15% at 200 and 280 nm.

Determination of the Rate Constants for the CH₃C(O)O₂ Self Reaction and for the CH₃C(O)O₂ Cross Reaction with

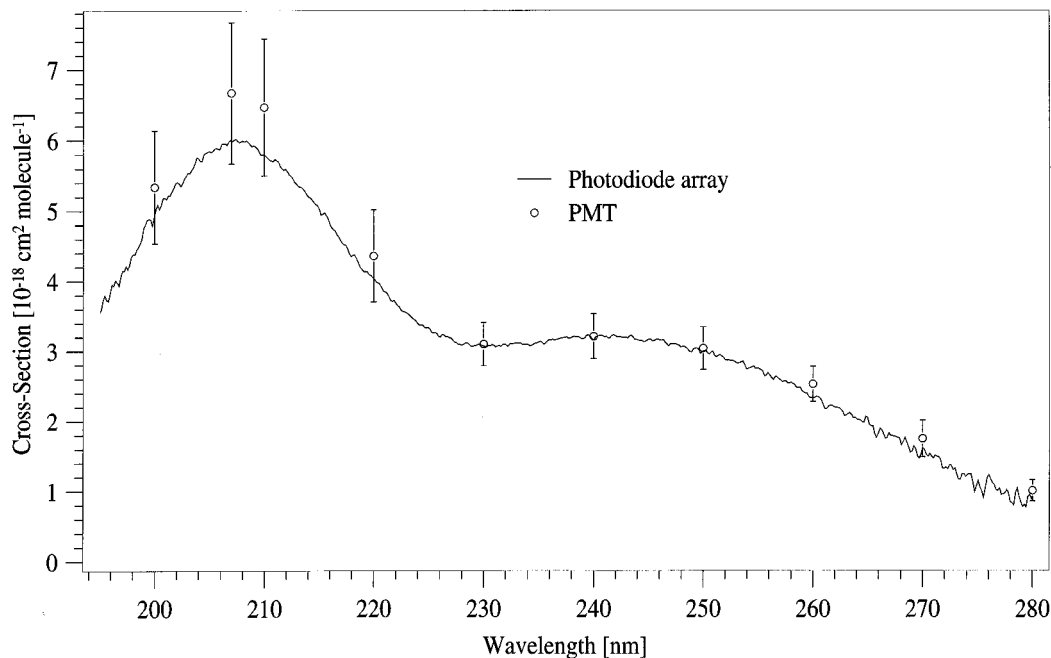


Figure 3. Comparison of the absolute (uncorrected) $\text{CH}_3\text{C}(\text{O})\text{O}_2$ absorption cross sections determined with the PMT (points) and the photodiode array (line).

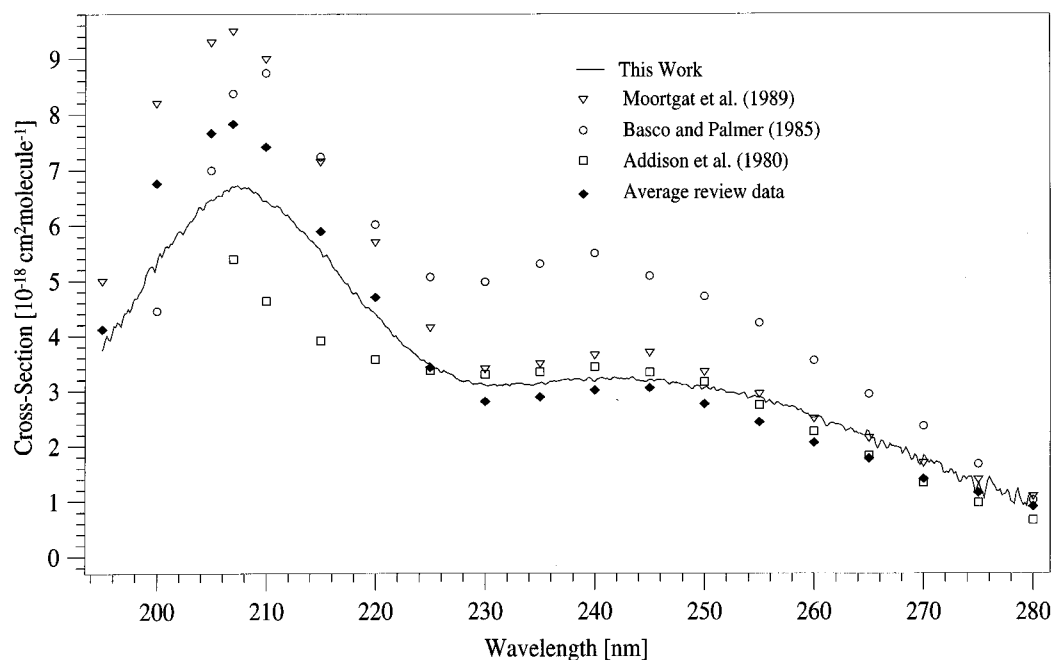


Figure 4. Comparison of the absolute $\text{CH}_3\text{C}(\text{O})\text{O}_2$ absorption cross sections measured here (solid line) and those of ref 7 (squares), ref 8 (circles), and ref 9 (triangles). The ref 9 spectrum, reduced 17.5%, is given as the black diamonds. The absorption cross sections reported here were corrected for a nonlinearity in the photodiode array detector, as described in the text.

CH_3O_2 . To determine the $\text{CH}_3\text{C}(\text{O})\text{O}_2$ self reaction rate constant, it was first necessary to deduce the $\text{CH}_3\text{C}(\text{O})\text{O}_2$ concentrations over a particular reaction time period. Although the initial radical concentrations were easily obtained by extrapolating measured absorbance profiles back to $t = 0$ and by substituting these values into eq B, the derivation of $\text{CH}_3\text{C}(\text{O})\text{O}_2$ concentrations at times > 0 was slightly more complex, as a result of the presence of other absorbing species, namely CH_3O_2 and HO_2 .

The concentrations of n absorbers can be calculated as a function of time from absorbance measurements made at n different wavelengths, if the equations generated from the appropriate substitutions into eq C are linearly independent. The values of the $\text{CH}_3\text{C}(\text{O})\text{O}_2$, CH_3O_2 , and HO_2 cross sections at

TABLE 1: Absorption Cross Sections of $\text{CH}_3\text{C}(\text{O})\text{O}_2$ in Units of $10^{-18} \text{ cm}^2 \text{ molecule}^{-1}$

wavelength, nm	σ	wavelength, nm	σ
195	3.75	240	3.21
200	5.34	245	3.20
205	6.46	250	3.04
207	6.67	255	2.89
210	6.47	260	2.53
215	5.53	265	2.25
220	4.36	270	1.75
225	3.49	275	1.32
230	3.10	280	1.13
235	3.13		

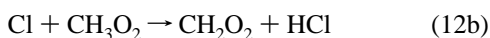
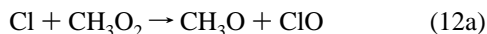
the wavelengths 210, 225, and 240 nm are unique, thus satisfying this criterion. An equation written generally as

$$\text{Abs}_t/l = \sigma(\text{CH}_3\text{C(O)O}_2)[\text{CH}_3\text{C(O)O}_2]_t + \sigma(\text{CH}_3\text{O}_2)[\text{CH}_3\text{O}_2]_t + \sigma(\text{HO}_2)[\text{HO}_2]_t \quad (\text{E})$$

was generated at each of the three wavelengths, and the concentrations of each absorber were calculated by simultaneously solving the three equations.

The absorption profiles, used in eq E, were obtained with the PMT in photolysis experiments performed on gaseous mixtures which can be divided into three categories according to the hydrocarbon concentration(s) used. In the first set of experiments, designated as “low CH₃CHO” data sets, CH₃CHO was the only hydrocarbon initially present and its concentration was $(3\text{--}30) \times 10^{14}$ molecule cm⁻³. CH₃CHO was again the only hydrocarbon initially present in the second set of measurements, called “high CH₃CHO”, but in these measurements the concentrations were about 2–3 orders of magnitude larger or $(2.1\text{--}3.5) \times 10^{17}$ molecule cm⁻³. CH₃C(O)O₂ and CH₃O₂ were simultaneously produced in the third set of measurements by adding CH₄ to the usual Cl₂/CH₃CHO/O₂ photolysis mixtures. Since H abstraction from CH₄, via reaction 11, is ~660 times slower than from CH₃CHO at 298 K, CH₃CHO concentrations were kept low, $(3\text{--}200) \times 10^{14}$ molecule cm⁻³, to further enhance the CH₃O₂ production. CH₄ concentrations were relatively high, $(2\text{--}7) \times 10^{18}$ molecule cm⁻³. The Cl₂ and O₂ concentrations were typically $(4\text{--}5) \times 10^{16}$ and $(0.6\text{--}1.0) \times 10^{19}$ molecule cm⁻³, respectively, throughout all measurements, yielding radical concentrations of $(2\text{--}5) \times 10^{13}$ molecule cm⁻³.

The newly measured absorption cross sections for CH₃C(O)O₂ were utilized in eq E, along with CH₃O₂ and HO₂ cross sections also measured with our flash photolysis/PMT system. The CH₃O₂ and HO₂ measurements were made relative to C₂H₅O₂, and the cross sections were calculated in the same manner as previously described for the CH₃C(O)O₂ cross sections. Because the reactions



were recently shown to be very rapid at room temperature,¹⁸ $k_{12} = (1.5 \pm 0.2) \times 10^{-10}$ cm³ molecule⁻¹ s⁻¹, and therefore potentially problematic to CH₃O₂ cross section determinations, special care was taken to ensure that the CH₄ concentration was sufficiently high. Measurements conducted with various initial CH₄ concentrations (ranging from 8×10^{17} to 2×10^{18} molecule cm⁻³) yielded virtually identical cross sections, indicating that the Cl + CH₃O₂ reaction was negligible under our experimental conditions. The remeasured cross sections of CH₃O₂ and HO₂ are listed in Table 2. Examples of typical measured absorption–time profiles and the corresponding concentration–time profiles, derived from the absorption–time profiles, the cross sections in Table 2, and eq E are shown in Figure 5.

A concentration decay profile of CH₃C(O)O₂ as a function of time reflects not only the self reaction loss of CH₃C(O)O₂, but also losses due to cross reactions. It is therefore not adequate to simply perform a second order fit to the CH₃C(O)O₂ decay curve to determine the self reaction rate constant. Instead, the FACSIMILE program of Harwell,¹⁹ which uses numerical techniques to solve differential chemical reaction equations, was employed. Each FACSIMILE input file consisted of the three absorbance profiles measured at 210, 225, and 240 nm, the initial gas concentrations (i.e., Cl₂, CH₃CHO, and O₂), initial CH₃C(O)O₂ radical concentrations (calculated from simple fits of the CH₃C(O)O₂ concentration profiles), the

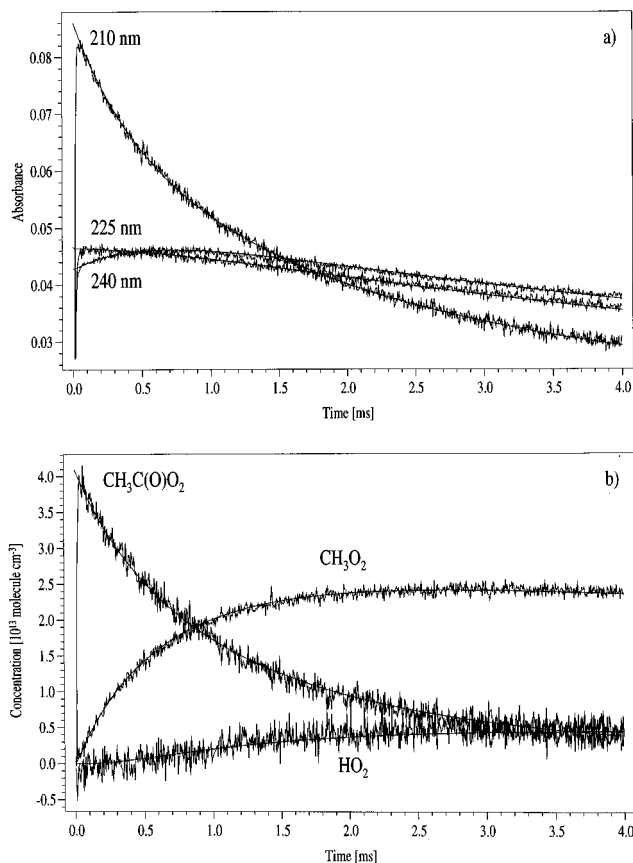


Figure 5. Examples of typical (a) measured absorption–time profiles and (b) concentration–time profiles calculated from the absorption–time profiles in (a). “Low acetaldehyde” conditions were used; $[\text{O}_2]_i = 5.7 \times 10^{18}$ molecule cm⁻³ and $[\text{Cl}_2]_i = 5.0 \times 10^{16}$ molecule cm⁻³. The solid lines are simulated by FACSIMILE from parameters obtained in the absorption data fitting.

TABLE 2: Absorption Cross Sections of CH₃C(O)O₂, CH₃O₂, and HO₂ Measured Here and Used in the FACSIMILE Fits and Simulations in Units of 10⁻¹⁸ cm² molecule⁻¹

wavelength, nm	$\sigma(\text{CH}_3\text{C(O)O}_2)$	$\sigma(\text{CH}_3\text{O}_2)$	$\sigma(\text{HO}_2)$
210	6.47	1.97	4.19
225	3.49	3.50	2.94
240	3.21	4.12	1.24

chemical mechanism and associated rate constants given in Table 3, the cross sections given in Table 2, and the wavelength specific absorbance equations (i.e., eq E). Selected parameters, usually one or more rate constants, were allowed to vary while the FACSIMILE program simultaneously fit the three absorbance profiles from 0 to 4 ms. As seen in Figure 5b, the CH₃C(O)O₂ concentration is nearly zero at 4 ms, indicating that most of the CH₃C(O)O₂ chemistry is over within that time period.

The rate constants k_1 , k_{4a} , and k_{4b} were allowed to vary simultaneously during initial fits, while all other parameters were held constant. Excellent fits were achieved with the “low CH₃CHO” data sets, and $k_1 = (1.36 \pm 0.02) \times 10^{-11}$ cm³ molecule⁻¹ s⁻¹, $k_{4a} = (8.4 \pm 0.2) \times 10^{-12}$ cm³ molecule⁻¹ s⁻¹, and $k_{4b} = (8.2 \pm 0.2) \times 10^{-13}$ cm³ molecule⁻¹ s⁻¹ were determined by averaging the fit results. The errors given here represent the standard deviation of the various measurements. Absorbance fits at wavelengths 210, 225, and 240 nm and the corresponding CH₃C(O)O₂, CH₃O₂, and HO₂ concentration simulated using the fitted parameters are compared to the measured absorbances, and calculated concentrations from a typical “low CH₃CHO” data set in Figure 5.

TABLE 3: Reaction Mechanisms and Rate Constants Used in FACSIMILE Fits and Simulations (First Order Rate Constants in Units of s⁻¹; Second Order Rate Constants in Units of cm³ molecule⁻¹ s⁻¹)

2CH ₃ C(O)O ₂ → 2CH ₃ C(O)O + O ₂	varied	
CH ₃ C(O)O + M → CH ₃ + CO ₂ + M	2.2E+5	estd
CH ₃ + O ₂ + M → CH ₃ O ₂ + M	9.2E-13	ref 20, 390 Torr, 298 K
CH ₃ C(O)O ₂ + CH ₃ O ₂ → CH ₃ C(O)O + CH ₃ O + O ₂	varied	
CH ₃ C(O)O ₂ + CH ₃ O ₂ → CH ₃ C(O)OH + HCHO + O ₂	varied	
CH ₃ C(O) + O ₂ + M → CH ₃ C(O)O ₂ + M	5.0E-12	estd from ref 1
CH ₃ O + O ₂ → HCHO + HO ₂	1.9E-15	ref 20
CH ₃ O ₂ + CH ₃ O ₂ → CH ₃ O + CH ₃ O + O ₂	1.2E-13	ref 10
CH ₃ O ₂ + CH ₃ O ₂ → HCHO + CH ₃ OH + O ₂	2.5E-13	ref 10
CH ₃ C(O)O ₂ + HO ₂ → CH ₃ C(O)OOH + O ₂	1.0E-11	refs 10, 14
CH ₃ C(O)O ₂ + HO ₂ → CH ₃ C(O)OH + O ₃	0.4E-11	refs 10, 14
HO ₂ + HO ₂ + M → H ₂ O ₂ + O ₂ + M	2.3E-12	ref 20, 390 Torr 298 K
HO ₂ + CH ₃ O ₂ → CH ₃ OOH + O ₂	5.8E-12	ref 10
Cl + CH ₃ CHO → CH ₃ C(O) + HCl	6.6E-11	ref 21
CH ₃ C(O) + Cl ₂ → CH ₃ C(O)Cl + Cl	1.0E-11	ref 21
Cl + CH ₄ → CH ₃ + HCl	1.0E-13	ref 20

TABLE 4: Sensitivity Calculations for k_1 , k_{4a} , and k_{4b} in Units of 10⁻¹¹, 10⁻¹², and 10⁻¹³ cm³ molecule⁻¹ s⁻¹, respectively^a

rate constant or cross sections varied	error range	$k_1(+,-)$	$k_{4a}(+,-)$	$k_{4b}(+,-)$
2CH ₃ C(O)O ₂ → 2CH ₃ C(O)O + O ₂	±0.2E-11	-, -	9.57, 7.23	4.71, 13.5
2CH ₃ O ₂ → CH ₃ O + CH ₃ O + O ₂	±0.2E-13	1.38, 1.38	8.54, 8.54	8.47, 8.26
2CH ₃ O ₂ → HCHO + CH ₃ OH + O ₂	±0.3E-13	1.38, 1.38	8.54, 8.54	8.68, 8.26
CH ₃ C(O)O ₂ + HO ₂ → CH ₃ C(O)OOH + O ₂	±0.4E-11	1.41, 1.37	9.09, 8.00	8.77, 8.13
CH ₃ C(O)O ₂ + HO ₂ → CH ₃ C(O)OH + O ₃	±0.3E-11	1.41, 1.37	8.98, 8.12	8.47, 8.16
2HO ₂ + M → H ₂ O ₂ + O ₂ + M	±0.6E-12	1.38, 1.38	8.54, 8.54	8.26, 8.26
HO ₂ + CH ₃ O ₂ → CH ₃ OOH + O ₂	±0.8E-12	1.38, 1.38	8.77, 8.54	8.47, 8.26
absolute CH ₃ O ₂ cross sections	±10%	1.31, 1.39	9.01, 5.43	27.6, -
absolute HO ₂ cross sections	±10%	1.42, 1.35	8.98, 8.07	8.68, 8.14
absolute CH ₃ C(O)O ₂ cross sections	±10%	1.55, 1.18	7.71, 5.86	-, 41.4
all absolute cross sections	±5%	1.49, 1.34	10.1, 8.90	10.9, 8.52

^a Typical data set refitted with one reaction rate constant or one set of σ varied within given error limits.

Analysis of the “high CH₃CHO” data sets yielded slightly different values, $k_1 = (1.51 \pm 0.03) \times 10^{-11}$, $k_{4a} = (5.3 \pm 2.4) \times 10^{-12}$, and $k_{4b} = (1.0 \pm 0.4) \times 10^{-12}$ cm³ molecule⁻¹ s⁻¹, with larger errors. Deviations from the measured absorbance curves were observed at times greater than about 1.5 ms, and acceptable fits were not attained with the simulations. Refitting the “high CH₃CHO” data sets up to only 1 ms resulted in better fits and an average rate constants of $k_1 = 1.37 \times 10^{-11}$ cm³ molecule⁻¹ s⁻¹, $k_{4a} = 8.3 \times 10^{-12}$ cm³ molecule⁻¹ s⁻¹, and $k_{4b} = 9.1 \times 10^{-13}$ cm³ molecule⁻¹ s⁻¹, in good agreement with the “low CH₃CHO” data sets. Secondary chemistry between CH₃CHO and CH₃C(O)O₂ or some product of the CH₃C(O)O₂ decomposition was suspected in these “high CH₃CHO” measurements, and attempts were made to refit these data, incorporating the reactions



The $K_{15}(\text{eq})$ was held fixed at 1×10^{-17} cm³ molecule⁻¹ (a value determined in ref 22) and the rate constants were allowed to vary during the fits; initial values, $k_{13} = 1.2 \times 10^{-16}$ cm³ molecule⁻¹ s⁻¹, $k_{14} = 1.5 \times 10^{-13}$ cm³ molecule⁻¹ s⁻¹, $k_{15} = 1.0 \times 10^{-15}$ cm³ molecule⁻¹ s⁻¹, and $k_{-15} = 100$ s⁻¹, were estimated from literature.²²⁻²⁴ Even though the agreement between the measured and FACSIMILE generated absorbance profiles at 210 nm was not perfect, the fits were greatly improved by the addition of reactions 14 and 15. The optimized fitted values were $k_{14} = 2.0 \times 10^{-13}$ cm³ molecule⁻¹ s⁻¹, $k_{15} = 3.8 \times 10^{-15}$ cm³ molecule⁻¹ s⁻¹, and $k_{-15} = 380$ s⁻¹. (Note: Because the fits were still not acceptable, these optimized parameters could be incorrect and, therefore, should be viewed

with caution.) Since k_{13} is so slow, it was undetermined by the data and is therefore unimportant in this system. Other reactions of CH₃CHO or the radical CH₃CH(OH)O₂ may explain the remaining discrepancy in the fits, but further investigations were not made here. Instead, the rate constants obtained from the “high CH₃CHO” data fits were not incorporated into the reported cross reaction rate constants.

For FACSIMILE fits performed on data sets with CH₄ added, k_1 was held at a constant 1.36×10^{-11} cm³ molecule⁻¹ s⁻¹ and only k_{4a} and k_{4b} were allowed to vary. k_1 should be better determined by the “low CH₃CHO” data, since the ratio of the CH₃C(O)O₂ radicals lost by self reaction to those lost by CH₃O₂ cross reactions is initially larger in the “low CH₃CHO” data sets than in systems with added CH₄. As before, the initial CH₃C(O)O₂ and CH₃O₂ concentrations were determined by fitting the respective concentration profiles (derived from eq E) back to time = 0. Best fit values of $k_{4a} = (9.1 \pm 2.1) \times 10^{-12}$ cm³ molecule⁻¹ s⁻¹ and $k_{4b} = (1.2 \pm 0.6) \times 10^{-12}$ cm³ molecule⁻¹ s⁻¹ were determined from these data.

Sensitivity Analysis. The errors given for k_1 , k_{4a} , and k_{4b} thus far reflect only the variation in these parameters as calculated by the FACSIMILE program. They do not take into account possible uncertainties in the input cross sections used to calculate the radical concentrations or in the “known” rate constants. To better understand which of these input parameters are the most influential in determining k_1 , k_{4a} , and k_{4b} , FACSIMILE runs were performed in which a particular rate constant or set of cross sections (see Table 4) was systematically varied within estimated error limits and a typical “low CH₃CHO” data set was refitted. The error limits of the rate constants were taken directly from the references given in Table 3 when possible. In cases where the branching ratio and rate constants were determined in separate studies, the error limits were calculated from the reported errors of each value. The effects of errors in the CH₃C(O)O₂ + CH₃O₂ rate constants on

k_1 were not evaluated since these rate constants depend on k_1 . Uncertainties in the absolute scales of the CH₃O₂ and HO₂ spectra of 10% were estimated from the maximum deviations between the cross sections measured here (Table 2) and the literature values.^{10,11,17,25} (See Discussion.) Possible errors due to incomplete Cl to radical conversion or unknown radical losses yielded an estimated uncertainty in the absolute scale of the CH₃C(O)O₂ spectrum of 10%. Finally, the effect of a C₂H₅O₂ calibration error was examined by varying the absolute cross sections of all absorbers $\pm 5\%$. The original fitted parameters for the particular "low CH₃CHO" data set used were $k_1 = 1.38 \times 10^{-11}$, $k_{4a} = 8.54 \times 10^{-12}$, and $k_{4b} = 8.26 \times 10^{-13}$ cm³ molecule⁻¹ s⁻¹, and the results are shown in Table 4.

The sensitivity calculations show, quite clearly, that k_1 is unaffected by the stated changes in the rate constants, indicating that errors in these rate constants will have little or no influence on the determination of k_1 . k_1 is sensitive to changes in the cross sections, and these fluctuations define the real error in the k_1 determination. A value of $k_1 = (1.36 \pm 0.19) \times 10^{-11}$ cm³ molecule⁻¹ s⁻¹ is hence concluded from this analysis. The largest variations in k_{4a} and k_{4b} coincide with changes in the fitted k_1 , suggesting that k_{4a} and k_{4b} are sensitive to changes in both the varied rate constant or cross sections and k_1 . Since the variations in k_{4a} and k_{4b} given in Table 4 are not independent of errors in k_1 , real errors in these rate constants cannot be assigned from this sensitivity analysis. Averaging the "low CH₃CHO" and "CH₄ added" results yields $k_{4a} = (8.8 \pm 1.5) \times 10^{-12}$ cm³ molecule⁻¹ s⁻¹ and $k_{4b} = (1.0 \pm 0.5) \times 10^{-12}$ cm³ molecule⁻¹ s⁻¹, where the quoted errors are the calculated standard deviations of measurements from both sets.

The possibility that our CH₃C(O)O₂ spectrum contains contributions from CH₃O₂ was also considered by adjusting the relative cross sections of CH₃C(O)O₂. If the CH₃C(O)O₂ had partially self reacted to form CH₃O₂ at the time of our measurements, then the shape of our CH₃C(O)O₂ spectrum would be altered; the shorter wavelength feature of the CH₃C(O)O₂ spectrum would be too low, the longer wavelength feature would be too high, and thus our $R = \sigma_{210\text{nm}}/\sigma_{240\text{nm}}$ ratio would be too low. The magnitude of error in this ratio would depend on the amount CH₃C(O)O₂ lost. For the sake of comparison, two runs were performed with $R = 2.5$, the $\sigma_{210\text{nm}}/\sigma_{240\text{nm}}$ ratio of the Moortgat *et al.*⁹ data, and either $\sigma_{240\text{nm}} = 3.21 \times 10^{-18}$ (this work) or $\sigma_{240\text{nm}} = 3.01 \times 10^{-18}$ (Moortgat *et al.*⁹ data rescaled down 17.5%). FACSIMILE was unable to fit the data using either set of parameters, suggesting that the 2.5 ratio is incorrect or that another parameter should simultaneously be changed in order to compensate. Due to the tremendous number of possible combinations, sensitivity tests with multiple parameter changes were not performed.

A generalized sensitivity analysis of all data sets obtained with added CH₄ was not possible because the fluxes through the various channels, and hence the sensitivities to these channels, varied with the initial CH₃C(O)O₂/CH₃O₂ concentrations. For measurements in which the CH₃O₂ concentration is low, the results should resemble those shown in Table 4, calculated in the absence of CH₄. As the CH₃O₂ concentration increases, the relative flux through reaction 4 will increase, while that through reaction 1 will decrease. At the same time, the absolute flux through the cross reaction channel will decrease because the CH₃C(O)O₂ concentration is being reduced. In addition, the influence of the CH₃O₂ self reactions will increase with the CH₃O₂ concentration and the fitted parameters, k_{4a} and k_{4b} , will become more sensitive to the values (or errors) of the CH₃O₂ self reactions.

Discussion

Absorption Cross Sections. A comparison of the CH₃C(O)O₂ spectrum obtained here and the previously measured spectra is shown in Figure 4. Also shown in Figure 4 is the Moortgat *et al.*⁹ spectrum scaled down 17.5%. (The scaling factor is an average of the recommended corrections given by the two recent peroxy radical reviews.^{10,11}) At wavelengths greater than 225 nm, our data are in reasonably good agreement with the averaged review data and the data of Addison *et al.*⁷ Large deviations in the shape and magnitude (as much as 19% at 207 nm) are noted when our data and those of Addison *et al.*⁷ are compared at wavelengths less than 225 nm, however, suggesting that the longer wavelength agreement between these two data sets is perhaps fortuitous. The absolute cross sections and relative peak heights of Basco and Parmar⁸ are notably different from ours. (It should be pointed out that the position of the shorter wavelength peak and its cross section are not exactly clear in the Basco and Parmar⁸ paper; in the text, the absorption maximum is cited to occur at 207 nm, while in their Figure 6, the spectrum is shifted toward longer wavelengths. Shown here are the values taken from their figure.) Even though our data most closely resembles the rescaled Moortgat *et al.*⁹ spectrum, the ratios $R = \sigma_{210\text{nm}}/\sigma_{240\text{nm}}$ still differ. Identical sources of CH₃C(O)O₂, namely the photolysis of Cl₂ in the presence of CH₃CHO and O₂, were employed in every study, so discrepancies between the data sets cannot be attributed to any systematic errors in the radical production mechanism.

Addison *et al.*⁷ did add NO₂ to the photolysis mixtures in order to scavenge the CH₃C(O)O₂ and 95% yields of PAN were reported. The absorption cross sections of PAN used in the spectral subtraction were determined in the same laboratory, but were not cited in the paper. The PAN data were said to be substantially confirmed by previously reported values of Stephens²⁶, which has since proven to be 20–30% too high.²⁷ Such an error would have a considerable effect in the CH₃C(O)O₂ spectrum, particularly in the short wavelength region, where the PAN cross sections are the largest.

A calibration error might explain the difference in the absolute scale of the Basco and Parmar⁸ spectrum, but this will not account for the disparity in ratio of the peak heights. The apparent mislabelling of the wavelength axis in their Figure 6 does create some uncertainty in the calculation of the peak height ratio; however, this uncertainty is too small to justify such a large difference. The presence of CH₃O₂ in their measurement could have resulted in a cross section at 240 nm that is too large. Calculations indicate that their initial CH₃C(O)O₂ radical concentration was an order of magnitude larger than ours, meaning that the decay rate of CH₃C(O)O₂ to produce CH₃O₂ was faster in their experiments. It is therefore possible that their CH₃C(O)O₂ spectrum contains some contribution of CH₃O₂.

Although rescaling the spectrum of Moortgat *et al.*⁹ does correct for the calibration error in initial CH₃C(O)O₂ concentrations, it does nothing to rectify the erroneously high HO₂ cross sections which were input parameters in the computer simulations of absorbance profiles. Furthermore, the CH₃O₂ cross sections used by Moortgat *et al.*⁹ also appear too high. The recommended CH₃O₂ cross sections^{10,11} are 5–8% lower than those employed by Moortgat *et al.*⁹ The effect of using incorrect cross sections in the simulations can best be understood by examining eq E (also used in Moortgat *et al.*⁹ simulations). The contribution of any one absorber to the total absorption ($\text{Abs}_{\lambda,i}$) is dependent on the product of the absorber's cross section and concentration; hence, the largest effects of incorrect cross sections will occur at wavelengths at which the cross sections of the particular absorber are large and over the time periods

when its concentration is large. The $\sigma(\text{HO}_2)$'s increase with decreasing wavelength, suggesting that errors in $\sigma(\text{HO}_2)$ might become important at shorter wavelengths. The overall influence of incorrect $\sigma(\text{HO}_2)$ on the simulations is expected to be small, however, since the HO_2 concentrations are low throughout the experiments and the shape of the absorbance profiles are primarily determined by $\text{CH}_3\text{C}(\text{O})\text{O}_2$ and CH_3O_2 . At wavelengths shorter than about 225 nm, the absorbance profiles closely resemble rapid second order decay curves of $\text{CH}_3\text{C}(\text{O})\text{O}_2$ since $\sigma(\text{CH}_3\text{C}(\text{O})\text{O}_2) \gg \sigma(\text{CH}_3\text{O}_2)$. Errors in the $\sigma(\text{CH}_3\text{O}_2)$ at these wavelengths are, therefore, not expected to introduce large errors in the simulations. At longer wavelengths though, the CH_3O_2 cross sections are larger than the $\text{CH}_3\text{C}(\text{O})\text{O}_2$ cross sections; the shapes of the absorbance profiles are strongly dependent on $\sigma(\text{CH}_3\text{O}_2)$ and actually appear to initially increase as the CH_3O_2 concentration increases. Simulations of the measured absorbance profiles conducted at longer wavelength, using $\sigma(\text{CH}_3\text{O}_2)$ values which are too high, are expected to result in $\sigma(\text{CH}_3\text{C}(\text{O})\text{O}_2)$ values which are too low. Due to the complexity of the fitting scheme, no attempt was made to resimulate the data.

Another possible problem in the Moortgat *et al.*⁹ work might have arisen from insufficient time resolution of their absorbance traces. Although it is not stated in their paper, it appears from the plots that the time resolution of their measurements was on the order of 50 μs . If the time resolution of the measurement is inadequate, the shape of the rapidly decreasing absorbance profiles at shorter wavelength will be distorted and the extrapolation to zero time will be incorrect. (Note: our data acquisition was a factor of 10 faster and hence should have a smaller error associated with it.) Of course the curvature in the absorbance trace depends not only on the wavelength of the measurement, but also on the initial $\text{CH}_3\text{C}(\text{O})\text{O}_2$ concentration. Initial radical concentrations of Moortgat *et al.*⁹ were around 1.1×10^{14} molecule cm^{-3} , a factor of 2.2–5.5 larger than the concentrations used here.

Finally, examination of Moortgat *et al.*⁹ absorption traces reveals that negative dips directly follow the flashes and that absorbances do not reach an immediate maximum. The length of their flash pulse (not stated in their paper) is assumed to be much longer than our laser flash and perhaps the detector does not fully recover from the influence of the flash lamp. Determinations of the initial $\text{CH}_3\text{C}(\text{O})\text{O}_2$ concentrations might be affected by the long delay in the signal recovery.

Rate Constants: k_1 , k_{4a} , and k_{4b} . As was demonstrated by the sensitivity analysis, correct cross sections of all absorbers are critical to the determination of accurate rate constants. In the hopes of eliminating systematic differences resulting from monochromator resolution, path length, etc., the CH_3O_2 and HO_2 cross sections were remeasured along with the $\text{CH}_3\text{C}(\text{O})\text{O}_2$ rather than being taken from the literature. The CH_3O_2 cross sections measured in this work are 10% lower than the recommended values of Lightfoot *et al.*¹⁰ however, they clearly lie within the range of data used in arriving at this recommendation ($\sigma_{240\text{nm}}$ ranged from 4.03 and 4.97×10^{-18} cm^2 molecule⁻¹). Our values are only 7% lower than the Wallington *et al.*¹¹ recommendations. Since the reviews were published, two new CH_3O_2 spectra have been reported^{17,25} with $\sigma(240\text{nm}) = 4.40$ and 4.22×10^{-18} cm^2 molecule⁻¹, which support our lower values. The HO_2 data measured here are in excellent agreement with the recommended values of Lightfoot *et al.*,¹⁰ varying less than 1% at 210 nm, but are about 8% lower than the recommended cross sections of Wallington *et al.*¹¹ It should be pointed out, however, that the Wallington *et al.*¹¹ recommendation included several older data sets which have noted

experimental flaws and excluded three measurements from 1991, which had not yet been published.

The $\text{CH}_3\text{C}(\text{O})\text{O}_2$ self reaction rate constant k_1 determined in the analysis of the "low CH_3CHO " data sets is in perfect agreement with that obtained from the "high CH_3CHO " data sets when the latter data sets are only fit to 1 ms. Secondary chemistry between CH_3CHO and products of the $\text{CH}_3\text{C}(\text{O})\text{O}_2$ decomposition seems likely in the "high CH_3CHO " measurements and explains the deviations in the fits at times greater than 1 ms.

The k_{4a} and k_{4b} obtained from the "low CH_3CHO " data sets are lower than those from measurements with added CH_4 by a factor of 1.1 and 1.5, respectively. Although the errors on the "low CH_3CHO " values are smaller, fits of these experiments are not expected to be as sensitive to the cross reaction rate constants as fits of the experiments with added CH_4 . Since CH_3O_2 is regenerated in reactions 2 and 3, there is no net change in CH_3O_2 concentration due to reaction 4a and k_{4a} is solely determined by changes in the $\text{CH}_3\text{C}(\text{O})\text{O}_2$ concentrations, after the loss due to the dominating self reaction is accounted for. Reaction flux calculations conducted with typical "low CH_3CHO " conditions have shown that reaction 4a only becomes competitive with reaction 1 at times greater than 1.5 ms and at that point the reaction flux through reaction 4a is small. Also, even though reaction 4b is derived from changes in both CH_3O_2 and $\text{CH}_3\text{C}(\text{O})\text{O}_2$ concentrations, the rate constant is relatively small and reaction 4b remains a minor channel throughout the entire reaction time period. Initial production of CH_3O_2 by the addition of CH_4 increases the flux through the cross reaction, and hence, the sensitivity to the cross reaction rate constant is expected to be greater.

The large error associated with the CH_4 added data was unanticipated, but can perhaps be explained by changes in the relative CH_3CHO and CH_4 concentrations, and thus the ratio of initial radical concentrations, during the course of the measurements. Small changes in the absorbance profiles could have been masked in the noise of the individual data sets of 500 laser pulses used in the final averaging. In the "low CH_3CHO " sets, the initial $\text{CH}_3\text{C}(\text{O})\text{O}_2$ concentrations only depend on the Cl concentration (and laser power) and slight changes in the CH_3CHO concentration, which is in excess over the Cl, would have no effect.

Due to the limitations of each of the data sets (both with and without CH_4) discussed above, neither set was preferred over the other and the final rate constants k_{4a} and k_{4b} were derived from averaging both the "low CH_3CHO " and " CH_4 added" results. Our $k_4 = (9.8 \pm 2.0) \times 10^{-12}$ cm^3 molecule⁻¹ s⁻¹ does fall within the error limits of the most recent measurement by Lesclaux *et al.*,¹⁵ $k_4 = (7.6 \pm 3.8) \times 10^{-12}$ cm^3 molecule⁻¹ s⁻¹. It should be noted, however, that the branching ratio employed by Lesclaux *et al.*¹⁵ was assumed to be $k_{4a}/k_4 = 0.48$, as determined earlier by Moortgat *et al.*⁹ A branching ratio of $k_{4a}/k_4 = 0.90 \pm 0.24$ was obtained in this study in good agreement with the most recently quoted value of $k_{4a}/k_4 = 0.83 \pm 0.17$ by Horie and Moortgat.¹⁴ Different $\text{CH}_3\text{C}(\text{O})\text{O}_2$ cross sections were used in the older works of Addison *et al.*,⁷ Basco and Parmar,⁸ and Moortgat *et al.*,⁹ and thus agreement between the rate constants determined in this work and theirs is coincidental at best. Different cross sections would mean different concentration profiles and, therefore, different rate constants, indicating that comparisons between our rate constant and those of the above-mentioned works, as such, are not meaningful.

Using the temperature dependence of the relative cross reaction rate constants of Horie and Moortgat¹⁴ $\beta = k_{4a}/k_{4b} =$

$2.2 \times 10^6 \exp(-3870/T)$ and our $k_4 = (9.8 \pm 2.0) \times 10^{-12} \text{ cm}^3 \text{ molecule}^{-1} \text{ s}^{-1}$, the temperature dependent rate constants can be calculated:

$$k_{4a} = 9.8 \times 10^{-12} / (1 + (1/2.2 \times 10^6 \exp(-3870/T))) \quad (\text{F})$$

$$k_{4b} = 9.8 \times 10^{-12} / (2.2 \times 10^6 \exp(-3870/T) + 1) \quad (\text{G})$$

These equations are valid only over the temperatures (263–333 K) used in ref 14 and with the value $k_4 = 9.8 \times 10^{-12} \text{ cm}^3 \text{ molecule}^{-1} \text{ s}^{-1}$, assuming k_4 is independent of temperature as suggested in ref 9.

Conclusions

A laser flash photolysis experiment was used to measure the ultraviolet absorption spectrum of acetylperoxy radical in the 195–280 nm range. The spectrum is bimodal, with a strong maximum at 207 nm, $\sigma = 6.67 \times 10^{-18} \text{ cm}^2 \text{ molecule}^{-1}$, and a weaker maximum near 240 nm, $\sigma = 3.21 \times 10^{-18} \text{ cm}^2 \text{ molecule}^{-1}$. CH₃O₂ and HO₂ cross sections were remeasured as a part of this study at several wavelengths within the range mentioned above. The values $\sigma_{240\text{nm}}(\text{CH}_3\text{O}_2) = (4.12 \pm 0.41) \times 10^{-18} \text{ cm}^2 \text{ molecule}^{-1}$ and $\sigma_{210\text{nm}}(\text{HO}_2) = (4.19 \pm 0.42) \times 10^{-18} \text{ cm}^2 \text{ molecule}^{-1}$ were obtained. A rate constant of $(1.36 \pm 0.19) \times 10^{-11} \text{ cm}^3 \text{ molecule}^{-1} \text{ s}^{-1}$ was determined for the acetylperoxy self reaction at 298 K, using the newly obtained cross sections, absorption–time profiles, and the FACSIMILE program. Rate coefficients of $k_{4a} = (8.8 \pm 1.5) \times 10^{-12} \text{ cm}^3 \text{ molecule}^{-1} \text{ s}^{-1}$ and $k_{4b} = (1.0 \pm 0.5) \times 10^{-12} \text{ cm}^3 \text{ molecule}^{-1} \text{ s}^{-1}$ were similarly determined for the acetyl- and methylperoxy cross reactions. The resulting k_4 is in good agreement with the recent measurement of Lesclaux *et al.*,¹⁵ and the branching ratio (0.90) is close to that reported by Horie and Moortgat.¹⁴

Acknowledgment. The authors wish to thank Dr. R. Lesclaux for helpful comments on the manuscript. This work was supported by the Commission of the European Community as a part of Project EV5V-CT-0038 (LABVOC).

Note Added in Proof. While examining the literature for the manuscript, several printing errors were noted in Section III. B.3—Acetylperoxy radicals of the recent Lightfoot *et al.*¹⁰ review. First, $\sigma(205 \text{ nm})$ for ref 1 in Table III.12 should be deleted; no such measurement exists. Three cross sections of ref 2 are in error; the corrected values should be $\sigma(205 \text{ nm}) = 6.99$, $\sigma(207 \text{ nm}) = 8.37$, and $\sigma(230 \text{ nm}) = 4.97$. Finally, $\sigma(207 \text{ nm}) = 8.37 \times 10^{-18}$ of ref 2 is missing from the plot in Figure III.11. Since the acceptance of this work, the authors

have become aware of a similar study submitted recently to *J. Phys. Chem.* by Maricq and Szenté. The UV cross sections of CH₃C(O)O₂ and the CH₃C(O)O₂ + CH₃O₂ rate constants (k_4) presented here and in the Maricq and Szenté work are in excellent agreement, and the CH₃C(O)O₂ self-reaction rate constants (k_1) agree within the error limits. An unexplained discrepancy exists, however, between the branching ratios of k_4 determined in the two studies.

References and Notes

- (1) Atkinson, R. *Atmos. Environ.* **1990**, *24A*, 1.
- (2) Roberts, J. M. *Atmos. Environ.* **1990**, *24A*, 243.
- (3) Singh, H. B.; O'Hara, D.; Herlth, D.; Bradshaw, J. D.; Sandholm, S. T.; Gregory, G. L.; Sachse, G. W.; Blake, D. R.; Crutzen, P. J.; Kanakidou, M. A. *J. Geophys. Res.* **1992**, *D15*, 16511.
- (4) Platt, U.; LeBras, G.; Poulet, G.; Burrows, J. P.; Moortgat, G. *Nature* **1990**, *348*, 147.
- (5) Madronich, S.; Calvert, J. G. *J. Geophys. Res.* **1990**, *95*, 5697.
- (6) Madronich, S.; Chatfield, R. B.; Calvert, J. G.; Moortgat, G. K.; Veyret, B.; Lesclaux, R. *Geophys. Res. Lett.* **1990**, *17*, 2361.
- (7) Addison, M. C.; Burrows, J. P.; Cox, R. A.; Patrick, R. *Chem. Phys. Lett.* **1980**, *73*, 283.
- (8) Basco, N.; Parmar, S. S. *Int. J. Chem. Kinet.* **1985**, *17*, 891.
- (9) Moortgat, G. K.; Veyret, B.; Lesclaux, R. *J. Phys. Chem.* **1989**, *93*, 2362.
- (10) Lightfoot, P. D.; Cox, R. A.; Crowley, J. N.; Destriau, M.; Hayman, G. D.; Jenkin, M. E.; Moortgat, G. K.; Zabel, F. *Atmos. Environ.* **1993**, *26A*, 1.
- (11) Wallington, T. J.; Dagaut, P.; Kurylo, M. J. *Chem. Rev.* **1992**, *92*, 667.
- (12) Kenley, R. A.; Traylor, T. G. *J. Am. Chem. Soc.* **1975**, *97*, 4700.
- (13) Weaver, J.; Meagher, J.; Shortridge, R.; Heicklen, J. *J. Photochem.* **1975**, *4*, 341.
- (14) Horie, O.; Moortgat, G. K. *J. Chem. Soc., Faraday Trans.* **1992**, *88*, 3305, and personal communication.
- (15) Lesclaux, R.; Boyd, A.; Nozière, B.; Villenave, E. LABVOC Report, Project EV5V-CT91-0038: Second Annual Report, Aug 4, 1994.
- (16) Bauer, D.; Crowley, J. N.; Moortgat, G. K. *J. Photochem. Photobiol. A: Chem.* **1992**, *65*, 392.
- (17) Maricq, M. M.; Wallington, T. J. *J. Phys. Chem.* **1992**, *96*, 986.
- (18) Maricq, M. M.; Szenté, J. J.; Kaiser, E. W. *J. Phys. Chem.* **1994**, *98*, 2083.
- (19) Curtis, A. R.; Sweetenham, W. P. *AERE Rep. R-12805* **1987** (U.K. Atomic Energy Research Establishment).
- (20) DeMore, W. B.; Sander, S. P.; Golden, D. M.; Hampson, R. F.; Kurylo, M. J.; Howard, C. J.; Ravishankara, A. R.; Kolb, C. E.; Molina, M. J. *Chemical Kinetics and Photochemical Data for Use in Stratospheric Modeling*; Evaluation No. 11, JPL Publication 94-26; JPL: Pasadena, CA, 1994.
- (21) Mallard, W. G.; Westley, F.; Herron, J. T.; Hampson, R. F. *NIST Standard Reference Database 17*; NIST Chemical Kinetics Database—Version 6.0; NIST: Gaithersburg, MD, 1994.
- (22) Kelly, N.; Heicklen, J. *J. Photochem.* **1978**, *8*, 83.
- (23) Weaver, J.; Meagher, J.; Shortridge, R.; Heicklen, J. *J. Photochem.* **1975**, *4*, 341.
- (24) Moortgat, G. K.; Cox, R. A.; Schuster, G.; Burrows, J. P.; Tyndall, G. S. *J. Chem. Soc., Faraday Trans. 2* **1989**, *85*, 809.
- (25) Wallington, T. J.; Maricq, M. M.; Ellermann, T.; Nielsen, O. J. *J. Phys. Chem.* **1992**, *96*, 982.
- (26) Stephens, E. R. *Adv. Environ. Sci. Technol.* **1969**, *1*, 119.
- (27) Senum, G. I.; Lee, Y.-N.; Gaffney, J. S. *J. Phys. Chem.* **1984**, *88*, 1269.

JP9526298